Multi-crack imaging using nonclassical nonlinear acoustic method*

Zhang Lue(张 略), Zhang Ying(张 盈), Liu Xiao-Zhou(刘晓宙)†, and Gong Xiu-Fen(龚秀芬)

Key Laboratory of Modern Acoustics, Institute of Acoustics, Nanjing University, Nanjing 210093, *China*

(Received 12 November 2013; revised manuscript received 18 February 2014; published online 10 August 2014)

Solid materials with cracks exhibit the nonclassical nonlinear acoustical behavior. The micro-defects in solid materials can be detected by nonlinear elastic wave spectroscopy (NEWS) method with a time-reversal (TR) mirror. While defects lie in viscoelastic solid material with different distances from one another, the nonlinear and hysteretic stress–strain relation is established with Preisach–Mayergoyz (PM) model in crack zone. Pulse inversion (PI) and TR methods are used in numerical simulation and defect locations can be determined from images obtained by the maximum value. Since false-positive defects might appear and degrade the imaging when the defects are located quite closely, the maximum value imaging with a time window is introduced to analyze how defects affect each other and how the fake one occurs. Furthermore, NEWS-TR-NEWS method is put forward to improve NEWS-TR scheme, with another forward propagation (NEWS) added to the existing phases (NEWS and TR). In the added phase, scanner locations are determined by locations of all defects imaged in previous phases, so that whether an imaged defect is real can be deduced. NEWS-TR-NEWS method is proved to be effective to distinguish real defects from the false-positive ones. Moreover, it is also helpful to detect the crack that is weaker than others during imaging procedure.

Keywords: nonclassical nonlinear acoustics, nonlinear elastic wave spectroscopy, time reversal, multi-carcks imaging

PACS: 43.25.+y, 43.35.+d **DOI:** 10.1088/1674-1056/23/10/104301

1. Introduction

Recent research has shown that micro-defects in solid materials can be detected by combining the techniques of nonlinear elastic wave spectroscopy (NEWS)[1] and time-reversal (TR),[2–4] namely NEWS-TR when the NEWS process is the pre-treated one and TR-NEWS when the NEWS process is the post-treated one.[5] Preisach–Mayergoyz (PM) model was first proposed by Preisach[6] and Mayergoyz,[7] then it was introduced into acoustics for the nonlinear wave propagation.[8,9] Based on the time-reversal invariance of wave equation, TR method is introduced into acoustic applications in refocusing of the source when the propagating elastic wave is reversed in time and irradiated backwards. Although it was used only for non-attenuation and linear medium when put forward originally, lately TR method has been verified to be also suitable for the materials with nonlinear weak attenuation and highly localized nonlinearity.[10] By regarding the defects as additional sources that produce harmonics, this method is capable of focusing harmonics while the rest of the material remains linear.

The development and validation of NEWS-TR method have been studied by Goursolle,[11] in which one defect was detected and different filtering algorithms were compared using numerical methods. In Ulrich *et al.*'s work,[12] an experiment was developed to detect cracks using TR mirror, Barbieri and Meo brought forward the decomposition of the time-reversal operator (DORT)[13,14] and developed a method to discern the nature of the defect and also to image the multi-cracks. In our previous work, the feasibility of NEWS-TR method for micro-damage imaging was analyzed and the influence of frequency on the prediction of the cracks was discussed.[15]

In this paper, the method of maximum value imaging[16] and the method of maximum value imaging with a time window are used to obtain the images of two cracks in the viscoelastic solid materials separately. With these images, studies are carried out to analyze how the cracks affect each other. Furthermore, an improved method, namely NEWS-TR-NEWS, is put forward to distinguish a real defect from the false-positive ones.

2. Modeling method

As far as the propagation of sound waves in heterogeneous elastic solid material is concerned, the Cauchy equations of motion are[17]

$$\dot{v}_x = \frac{1}{\rho}\left(\frac{\partial \sigma_{xx}}{\partial x} + \frac{\partial \sigma_{xy}}{\partial y}\right) + F_x, \tag{1}$$

$$\dot{v}_y = \frac{1}{\rho}\left(\frac{\partial \sigma_{xy}}{\partial x} + \frac{\partial \sigma_{yy}}{\partial y}\right) + F_y. \tag{2}$$

The stress rate equations are[17]

$$\dot{\sigma}_{xx} = K_1\dot{\varepsilon}_{xx} + K_2\dot{\varepsilon}_{yy} = K_1\frac{\partial v_x}{\partial x} + K_2\frac{\partial v_y}{\partial y}, \tag{3}$$

*Project supported by the National Basic Research Program of China (Grant Nos. 2012CB921504 and 2011CB707902), the National Natural Science Foundation of China (Grant No. 11274166), the Funds from the State Key Laboratory of Acoustics, Chinese Academy of Sciences (Grant No. SKLA201401), and the China Postdoctoral Science Foundation (Grant No. 2013M531313).

†Corresponding author. E-mail: xzliu@nju.edu.cn

© 2014 Chinese Physical Society and IOP Publishing Ltd

$$\dot{\sigma}_{yy} = K_1\dot{\varepsilon}_{yy} + K_2\dot{\varepsilon}_{xx} = K_1\frac{\partial v_y}{\partial y} + K_2\frac{\partial v_x}{\partial x}, \tag{4}$$

$$\dot{\sigma}_{xy} = \mu(\dot{\varepsilon}_{xy} + \dot{\varepsilon}_{yx}) = \mu\left(\frac{\partial v_y}{\partial x} + \frac{\partial v_x}{\partial y}\right), \tag{5}$$

where v_x and v_y are the x and y components of particle velocity; σ_{xx}, σ_{yy}, and σ_{xy} are the stress components; F_x and F_y are the volume force densities determining the external action; K_1, K_2, and μ represent the elastic moduli respectively; ρ is the material density. To discretize Eqs. (1)–(5), the elastodynamic finite integration technique (EFIT)[18] is employed. Disregarding external force, the following equations can be obtained for the node (n, m) on an elementary mesoscopic cell:[17]

$$\dot{v}_x^{(n,m)}(t) = \frac{1}{\Delta}\frac{2}{(\rho^{(n,m)} + \rho^{(n+1,m)})}[\sigma_{xx}^{(n+1,m)}(t) - \sigma_{xx}^{(n,m)}(t) + \sigma_{xy}^{(n,m)}(t) - \sigma_{xy}^{(n,m-1)}(t)], \tag{6}$$

$$\dot{v}_y^{(n,m)}(t) = \frac{1}{\Delta}\frac{2}{(\rho^{(n,m)} + \rho^{(n,m+1)})}[\sigma_{yy}^{(n,m+1)}(t) - \sigma_{yy}^{(n,m)}(t) + \sigma_{xy}^{(n,m)}(t) - \sigma_{xy}^{(n-1,m)}(t)], \tag{7}$$

$$\dot{\sigma}_{xx}^{(n,m)}(t) = \frac{1}{\Delta}K_1^{(n,m)}[v_x^{(n,m)}(t) - v_x^{(n-1,m)}(t)] + \frac{1}{\Delta}K_2^{(n,m)}[v_y^{(n,m)}(t) - v_y^{(n,m-1)}(t)], \tag{8}$$

$$\dot{\sigma}_{yy}^{(n,m)}(t) = \frac{1}{\Delta}K_1^{(n,m)}[v_y^{(n,m)}(t) - v_y^{(n,m-1)}(t)] + \frac{1}{\Delta}K_2^{(n,m)}[v_x^{(n,m)}(t) - v_x^{(n-1,m)}(t)], \tag{9}$$

$$\dot{\sigma}_{xy}^{(n,m)}(t) = \frac{1}{\Delta}\frac{4}{\left(\frac{1}{\mu^{(n,m)}} + \frac{1}{\mu^{(n+1,m)}}\frac{1}{\mu^{(n,m+1)}}\frac{1}{\mu^{(n+1,m+1)}}\right)} \times [v_x^{(n,m+1)}(t) - v_x^{(n,m)}(t) + v_y^{(n+1,m)}(t) - v_y^{(n,m)}(t)], \tag{10}$$

where Δ is the square grid, i.e., $\Delta = \Delta x = \Delta y$.

In viscoelastic solid materials, the amplitude of sound waves will attenuate while propagating. A simplified model can be used to simulate such an attenuation, in which the stress and strain are multiplied at each time step with an attenuation factor defined as[19]

$$\alpha = \exp(-\pi f \Delta t/Q), \tag{11}$$

where f, Δt, and Q denote the source frequency, time step, and quality factor respectively.

Numerical simulation is carried out on a linear medium sample with defect whose geometry is indicated in Fig. 1. The relevant physical parameters are $\rho = 7700$ kg/m^3, $K_1 = 1.412 \times 10^{11}$ Pa, $K_2 = 5.2202 \times 10^{10}$ Pa, and $\mu = 4.45 \times 10^{10}$ Pa while the quality factor Q is 10. In Fig. 1, the source is located on the left side of the sample, ranging from 5 mm to 145 mm. The receiver is a one-dimensional array with a length of 148 mm and abscissa 225 mm. The defect is assumed to be a 10 mm $\times$ 7 mm rectangle area with hysteretic nonlinear behavior while the remaining part of the sample remains linear. Square grids used in numerical computation are 0.5 mm $\times$ 0.5 mm in time steps of 5×10^{-8} s, and the sampling rate is 20 MHz with the number of sample data 5000.

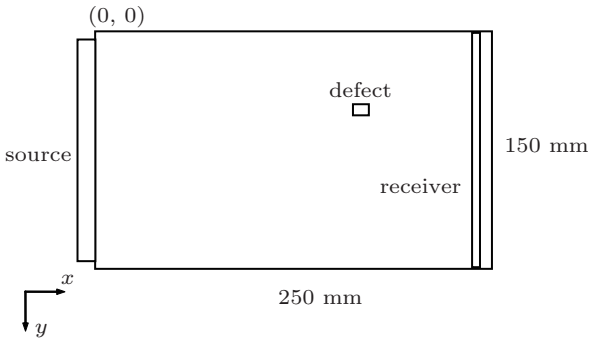


Fig. 1. Geometry of viscoelastic solid material sample with one defect.

Recent experiments on certain materials have shown that the cracked region generates not only odd harmonics but also even harmonics when excited.[20] As shown in Fig. 2, a modified PM model[11] is used to simulate this behavior. In the modified PM model, the initial state of hysteretic element is assumed to be open, and the hysteretic element represents linear elastic properties with modulus K_{M1} while the stress increases from P_o to P_c; when the stress leaps over P_c, the strain exhibits a step change with the threshold value r_2 and the hysteretic element turns into a closed state; then with stress increasing, the hysteretic element sequentially maintains linear elasticity with modulus K_{M2}. In case the stress decreases from a value more than P_c, the hysteretic element with an initially closed state will maintain linear elasticity with modulus K_{M2} until the stress becomes less than P_o; when the decreasing stress leaps over P_o, a step change of the strain with the threshold value r_1 occurs and the state of hysteretic element turns open. As stress decreases, the hysteretic element maintains linear elasticity with modulus K_{M1}. While preserving the characteristics of the odd harmonics from original PM model, even harmonics can be generated from the modified PM model, which describes the experimental observation better. In general, when the pore pressure increases ($\partial P/\partial t > 0$), the strain contribution ε_M of each hysteresis element is expressed as[11]

$$\frac{\partial \varepsilon_M}{\partial P} = -\frac{1}{K_{M1}},$$

if the hysteretic element is open,

$$\frac{\partial \varepsilon_M}{\partial P} = -\frac{1}{K_{M2}}, \tag{12}$$

if the hysteretic element is closed.

Subsequently, by defining $f(P_o, P_c)$ as the density distribution on the PM space, the strain contribution ε_H of all hysteresis elements is obtained by

$$\frac{\partial \varepsilon_H}{\partial P} = -\int_{O_2}^{P} dP_o r_2 f(P_o, P) - \frac{1}{K_{M2}} \int_{-\infty}^{P_c} dP_o \int_{P_0}^{+\infty} dP_c f(P_o, P_c) - \left(\frac{1}{K_{M1}} - \frac{1}{K_{M2}}\right) \int_{O_2}^{P_c} dP_o \int_{P}^{+\infty} dP_c f(P_o, P_c). \quad (13)$$

O_2 is the P_o value of the hysteresis element determined by the PM space. According to Goursolle *et al.*'s study,[11] in the above equation, the first double integral term is the inverse of the bulk modulus contribution when all the hysteresis elementary units are in the open state, the second double integral term represents the modification of the inverse of the bulk modulus due to closed hysteresis elements, and the single integral term represents the additional contribution to the inverse of the bulk modulus of the hysteresis elementary units opening at the actual pore pressure P. Similarly, when the pore pressure decreases the following equation is obtained:

$$\frac{\partial \varepsilon_H}{\partial P} = -\int_{P}^{C_2} dP_c r_1 f(P, P_c) - \frac{1}{K_{M1}} \int_{-\infty}^{P_c} dP_o \int_{P_0}^{+\infty} dP_c f(P_o, P_c) - \left(\frac{1}{K_{M2}} - \frac{1}{K_{M1}}\right) \int_{-\infty}^{P_c} dP_o \int_{P_0}^{C_2} dP_c f(P_o, P_c), \quad (14)$$

where C_2 is the P_c value of the hysteresis element determined by the PM space. Combining Eqs. (13) and (14) with the finite integration equations listed above, the hysteresis relation between modulus and stress is modeled in the defected region and the numerical solutions that contain harmonic components are obtained.

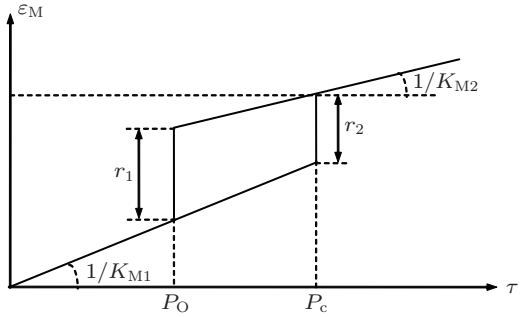


Fig. 2. Hysteretic element of modified PM model.

In this paper, the sample is excited by a continuous source, and the external force applied is implemented as $F_x = A\sin(2\pi ft)$ and $F_y = 0$, where $A = 1 \times 10^8$ and the exciting frequency $f = 250$ kHz. The maximum value imaging procedure[16] is applied to TR process. According to this imaging procedure, we define the function $v_x(x, y; t)$, which describes a component of particle velocity at (x, y) position and time t. $M(x,y) = \max[v_x(x,y;t)]$ is defined as the maximum value of v_x. M is expected to present the maximum wherever the focusing occurs, together with the secondary maximum where the unfocused paths from the N receivers interfere coherently toward the focusing point. After the identification of ray paths, the matrix M is utilized to obtain the maximum value image. Through this imaging procedure, both the focal point and the ray path of sound wave can be identified. It should be noticed that the maximum value imaging with a time window is applied to the wave field over a certain period of time in this work. Afterwards, a PI filter[20] is employed to extract the nonlinear components of the signals acquired by receivers. Compared with traditional harmonic filtering, the PI procedure has been proved to be more robust and reliable in damage image[20] under various conditions. PI procedure is especially capable of detecting the defect near the edge of the sample while the harmonic filtering fails, due to the residual of fundamental frequency when using traditional harmonic filtering.

3. Numerical results and discussion

In numerical computation, the signals acquired by receivers are time-reversed and then emitted by the receivers. When there is only one crack in the sample, it can be shown quite clearly in the image obtained through the maximum value imaging no matter where the crack is located. Defect image of the sample shown in Fig. 1 is presented in Fig. 3, in which the area surrounded by the black line refers to the actual location of the defect.

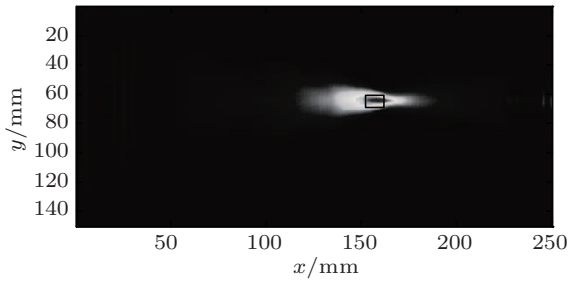


Fig. 3. Defect image of a sample with one defect whose center is located at (157.5, 64).

Subsequently, the condition of two defects lying in the sample is considered. Cracks can be clearly imaged if the distance between their centers is more than 25 mm when 250 kHz is chosen as an exciting frequency as indicated in Fig. 4, while false-positive cracks may occur for smaller distance (shown in Fig. 5). The false-positive cracks will disappear when the exciting frequency is increased. If the exciting frequency is chosen to be 700 kHz, for instance, the defects can still be distinguished by imaging without the occurrence of false-positive

cracks if the distance between their centers is no less than 5 mm. However, once the exciting frequency is chosen to be much higher, the particle velocity will become too small to be detected by the receiver. According to Eq. (11), for viscoelastic solid materials, attenuation grows as the exciting frequency is increased. For excitations at different frequencies, the nonlinear response of defects can be represented by the amplitude of signal power spectrum. In other words, the nonlinear response is weak when the amplitude of signal power spectrum is small, which may lead to omissions while recognizing defects. Thus, increasing exciting frequency is not a practical way to pursue a better image and it is still necessary to work out the causation of false-positive defects and then to distinguish false-positive defects from the real ones.

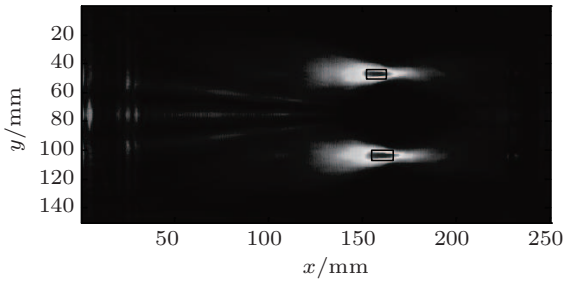


Fig. 4. Defect image of a sample with two defects whose center locations are at (157.5, 103.5) and (157.5, 46.5) respectively.

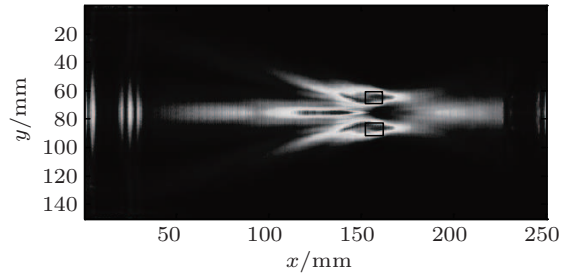


Fig. 5. Defect image of a sample with two defects whose center locations are at (157.5, 64) and (157.5, 86) respectively.

In the occasion that two defects are located closely to each other in the solid material, two typical situations are studied: the abscissas or the longitudinal coordinates of the centers of the two defects are the same. For the first situation, positions of the defects' centers are set to be at (157.5, 64) and (157.5, 86). Figure 5 shows the maximal imaging of this situation, in which the maximal velocities are observed at positions (157, 64) and (158, 86) respectively, with a relatively small error compared with the preset defects' centers. Thus, the maximum value imaging is proved to be valid to detect the two cracks that are located closely to each other. Nevertheless, another bright area indicated in Fig. 5 can also be seen, which might be regarded as a third defect in the sample, i.e., a false-positive defect. To study how this false-positive defect occurs, the maximum value imaging with a time window is then applied. In this method, the maximum value imaging over a chosen time interval Δt from the starting time t_{R} is used and the signal is analyzed. Taking starting time $t_{\mathrm{R}} = 0.2177$ ms and time window $\Delta t = 6.25 \times 10^{-4}$ ms, as observed in Fig. 6, the area of the false-positive defect is where the wave fronts of the harmonics generated by different defects meet. As a matter of fact, after focusing around the positions of defects, the sound wave will continue propagating and its wave front will spread. If the defects are located close to each other, the wave fronts of different waves will overlap at a certain position. And if the phases of the sound waves are not opposite, the amplitudes of waves will be added to each other at that position. Then a higher particle velocity at this location can be expected, which explains how the false-positive defect is generated.

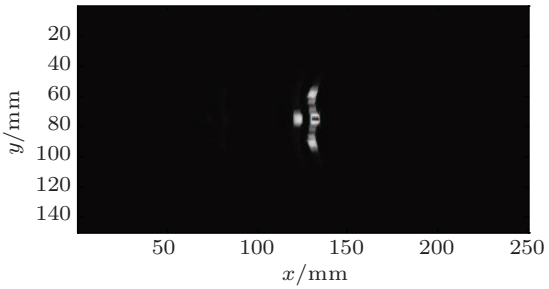


Fig. 6. Defect image for two defects whose center locations are at (157.5, 64) and (157.5, 86) with a time window staring from 0.2177 ms.

Because of the false-positive defect, the shapes of defects in Fig. 4 are quite different from those in Fig. 5. The difference between Fig. 5 and Fig. 3 is significant even though one of the defects in each of both cases has the same size and location. It can be inferred that the change of harmonics in Fig. 5 is due to the existence of the second defect. To prove this inference, the method of maximum value imaging with a time window is applied to the two conditions mentioned above with the time window $\Delta t = 6.25 \times 10^{-4}$ ms and starting time $t_{\mathrm{R}} = 0.2375$ ms, and corresponding results are presented in Figs. 7(a) and 7(b). After focusing at the area of the upper defect, while the wave front remains in Fig. 7(a), the wave front of harmonics in Fig. 7(b) splits into two parts: one is propagating along the x axis and the other is propagating obliquely. Meanwhile, the shapes of wave front in the two figures are also quite different. In a word, the procedure of the production and the propagation of harmonics in one damage zone will be affected by another damage nearby.

For the second case that longitudinal coordinates of two defect centers are the same, e.g., (117.5, 75) and (147.5, 75), corresponding images are shown in Fig. 8 where the positions of the maximal velocity are at (118, 74.5) and (151, 75) respectively. Number the defects with smaller value of abscissa and denote them as Defect 1 and denote the remaining defects as Defect 2, then number the harmonics produced by Defect 1

and denote them as Harmonics 1 and the harmonics produced by Defect 2 as Harmonics 2 for convenience. The existence of two bright areas on the side of defects is due to the fact that in TR process, the harmonics focusing at the area of Defect 2 and the harmonics focusing at the area of Defect 1 will meet in the two areas and overlap each other.

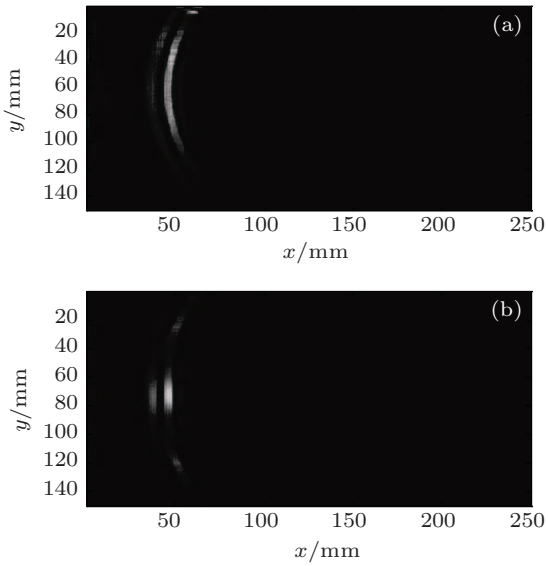


Fig. 7. Defect images for (a) one defect whose center location is at (157.5, 64) and (b) two defects whose center locations are at (157.5, 64) and (157.5, 86), with a time window starting from 0.2375 ms.

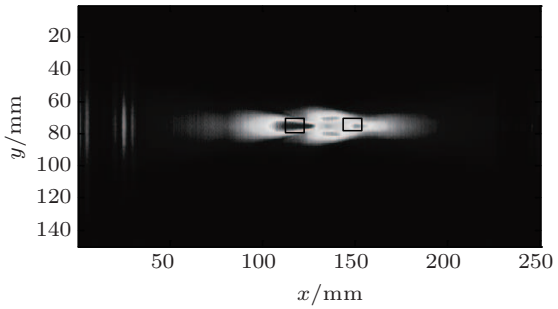


Fig. 8. Defect image of a sample with two defects whose center locations are at (117.5, 75) and (147.5, 75).

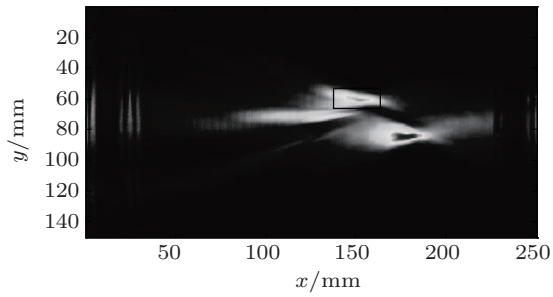


Fig. 9. Defect image of a sample with two defects whose centers are located at (147.5, 61.5) and (177.5, 83.5) respectively.

It can be seen that one of the defects is sometimes brighter than the other while imaging. This is due to the fact that one defect can block the nonlinearities induced by the other. In this situation, it is possible to ignore the weak defect in image obtained in the simulation. Taking two defects whose centers are located are respectively at (147.5, 61.5) mm and (177.5, 83.5) mm for example, the image in Fig. 9 indicates that neither the false-positive defect nor the real defect is as bright as the other one, which might lead to a neglect in recognition.

The above results have proved that the maximum value imaging with a time window method is valid to determine the false-positive defect when the abscissas of two defect centers are the same. However, the condition that the longitudinal locations of the defects are the same with respect to the excitation position does not hold true while using the maximum value imaging with a time window method. In addition, solutions need to be found for the accurate recognition of the weak defect after imaging.

In this work, a new scheme, namely NEWS-TR-NEWS scheme, is proposed to determine a false-positive defect and recognize a weaker defect in the image. Compared with NEWS-TR scheme, the NEWS-TR-NEWS scheme contains another nonlinear analysis procedure as a post-treatment of time reversal, which is shown in Fig. 10.

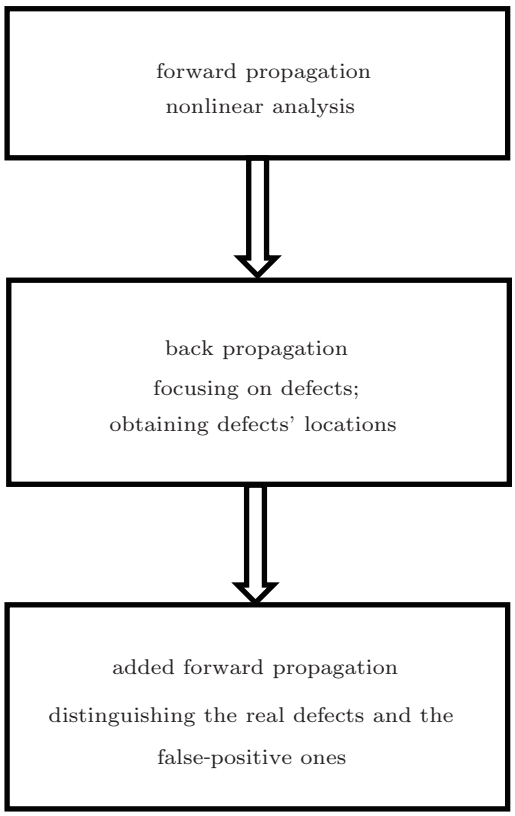


Fig. 10. Procedure of NEWS-TR-NEWS scheme.

According to the above discussion, the locations of defects centers can be determined by the maximum value imaging, including both the false-positive defects and the weaker ones. A laser vibrometer is used in the newly added forward propagation procedure to scan particle velocity along the

y direction at all the locations that have been obtained after NEWS-TR phase. To complete the second forward propagation, two forward signals with inverse phases need to be emitted into the sample and the corresponding nonlinear signal at a position can be acquired through PI filtering. For an arbitrary position in the sample, by making $x = x_k$ and $y = y_k$, its nonlinear signal can be obtained as a time serial, $v_x(t)$ and its maximum, $\max(v_x(t))$ is then extracted. If the receiver scans along the y direction, $M = \max(v_x(t))$ at these positions with regard to y is obtained, which can be utilized to determine whether an imaged defect is real or fake.

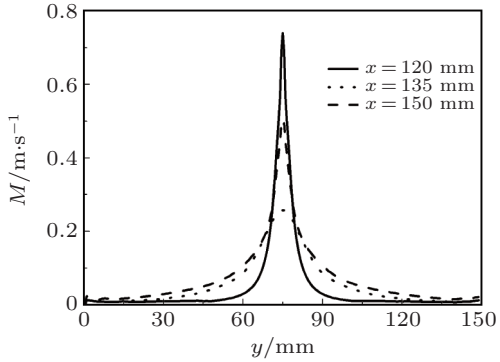


Fig. 11. Maximum velocity distributions along the y direction at $x = 120$ mm, $x = 135$ mm, and $x = 150$ mm for two defects whose centers are located at (117.5, 75) and (147.5, 75).

For a real defect that has been imaged, a peak can be expected in the figure because the nonlinear wave is generated from the cracked area and spreads gradually during its propagation. Its value reaches the maximum as it is generated in the defect area. On condition that the longitude coordinates of cracks are the same as those shown in Fig. 8, the positions to be scanned during the newly added forward propagation are $x_1 = 120$ mm, $x_2 = 135$ mm, and $x_3 = 150$ mm. According to the NEWS-TR-NEWS scheme, the M distribution along the y direction is obtained with the nonlinear signals received, as shown in Fig. 11, in which the expected peaks are observed at $x_1 = 120$ mm and $x_3 = 150$ mm. Since the peak value at $x_3 = 150$ mm is larger than that at $x_2 = 135$ mm, the former nonlinear signal is induced by a real defect at the location rather than the propagation of harmonics induced by the left defect. However, the expected two peaks do not appear at $x_2 = 135$ mm as shown in Fig. 8, the corresponding defects can be regarded as false-positive ones. The one peak at $x_2 = 135$ mm is due to the propagation of the harmonics generated at $x_1 = 120$ mm. On condition that the abscissas of the centers of the two defects are the same as those shown in Fig. 5, the receiver scans at $x_1 = 148$ mm and $x_2 = 158$ mm so that the nonlinear signals are obtained by NEWS-TR-NEWS scheme and the corresponding result is shown in Fig. 12. No significant peak is observed in Fig. 12(a) and the velocity is quite small, which implies that the defect imaged at $x_1 = 148$ mm in Fig. 5 is a false-positive one. On the other hand, two peaks exist just as indicated in Fig. 12(b), which means that two defects actually exist at $x_2 = 158$ mm. Nevertheless, in Fig. 9, one defect (surrounded by black line) seems to be much weaker than the other, thus it is difficult to say whether it indicates a real defect. In order to determine the exact number of defects in Fig. 9, scanning is taken by the receiver at $x_1 = 150$ mm, $x_2 = 178$ mm separately. Consequently, the similar results are obtained correspondingly as shown in Fig. 13 where a peak appears for $x = 178$ mm, which indicates that a defect really exists at the corresponding position.

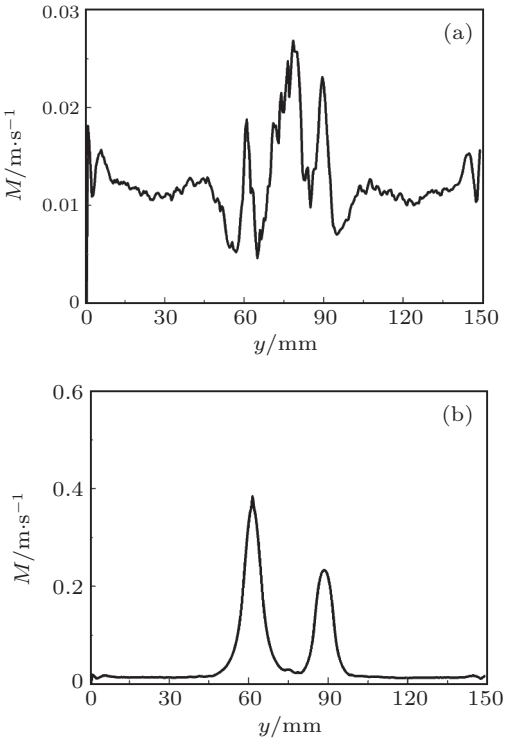


Fig. 12. Maximum velocity distributions along y direction at $x = 148$ mm (a) and 158 mm (b) for two defects whose centers are located at (157.5, 64) and (157.5, 86) respectively.

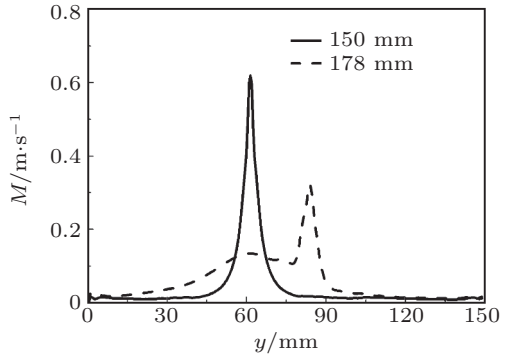


Fig. 13. Maximum velocity distributions along y direction at $x = 178$ mm and $x = 150$ mm for two defects whose center locations are at (147.5, 61.5) and (177.5, 83.5).

It should be noticed that inadequate spatial sampling can lead to the sidelobes and false judgment of defects even if there

is only one real defect in the solid specimen. Optimization of sampling scheme and array of transducers helps to improve these issues. Nevertheless, the occurrence of the false-positive defects mentioned above is mainly due to the small distances between defects. As a matter of fact, there is a constructive superposition of wave fronts during the propagating of all harmonics, which are expected to be refocused at their original defects after time reversal. A false-positive defect emerges when the transient vibration of such superposition is captured during the maximum value imaging.

4. Conclusion

The performance of the maximum value imaging method is satisfactory in most applications mainly for two reasons: firstly, it can help to determine the wave path during the back propagation of TR process; secondly, the image time is not involved in this method, which is actually quite difficult to determine directly. Nevertheless, the maximum value imaging method might lead to the occurrence of false-positive defects when the distance between defects is small. The maximum value imaging with a time window is introduced to explain how the defects affect each other and to determine whether the imaged ones are real defects. On the other hand, NEWS-TR-NEWS scheme is also proposed to distinguish the false-positive defects from the real ones, with another NEWS process added to the traditional NEWS-TR scheme. Numerical results have shown that the NEWS-TR-NEWS method is capable of not only recognizing the crack that is weaker than others during the imaging procedure, but also determining the cracks that are close to each other. However, when the distance between cracks is too small, it is not necessary to distinguish the exact crack number since they are permissible to be regarded as one. In future, experiments will be conducted to verify the numerical simulation results presented in this paper.

References

[1] Van Den Abeele K, Sutin A, Carmeliet J and Johnson P A 2001 *NDT & E Int.* **34** 239
[2] Fink M 1992 *IEEE Trans. Ultrason. Ferroelectr. Freq. Control* **39** 555
[3] Zhang H Y, Cao Y P, Sun X L, Chen X H and Yu J B 2010 *Chin. Phys. B* **19** 114301
[4] Zhang B X, Liu D D, Shi F F and Dong H F 2013 *Chin. Phys. B* **22** 014302
[5] Le Bas P, van den Abeele K, Dos Santos S, Goursolle T and Bou Matar O 2006 *European Conference on Non-Destructive Testing* (Berlin: German Society for Non-Destructive Testing)
[6] Preisach F 1935 *Z. Phys.* **94** 277
[7] Mayergoyz J D 1985 *J. Appl. Phys.* **57** 3803
[8] McCall K R and Guyer R A 1994 *J. Geophys. Res.* **99** 23887
[9] Guyer R A, McCall K R and Boitnott G N. 1995 *Phys. Rev. Lett.* **74** 3491
[10] Anderson B E, Griffa M, Larmat C, Ulrich T J and Johnson P A 2008 *Acoust. Today* **4** 5
[11] Goursolle T, Callé S, Dos Santos S and Bou Matar O 2007 *J. Acoust. Soc. Am.* **122** 3220
[12] Ulrich T J, Johnson P A and Guyer R A 2007 *Phys. Rev. Lett.* **98** 104301
[13] Barbieri E and Meo M 2010 *Wave Motion* **47** 452
[14] Barbieri E and Meo M 2010 *Int. J. Solids Struct.* **47** 2639
[15] Zhu J L, Zhang Y and Liu X Z 2014 *Wave Motion* **51** 146
[16] Gliozzi A S, Griffa M and Scalerandi M 2006 *J. Acoust. Soc. Am.* **120** 2506
[17] Vanaverbeke S and Van Den Abeele K 2007 *J. Acoust. Soc. Am.* **122** 58
[18] Fellinger P, Marklein R, Langenberg K J and Klaholz S 1995 *Wave Motion* **21** 47
[19] Graves R W 1996 *Bull. Seismol. Soc. Am.* **86** 1091
[20] Simpson D H, Chin C T and Burns P N 1999 *IEEE Trans. Ultrason. Ferroelectr. Freq. Control* **46** 372